energies

MDPI

Article

Influence of Raman Spectroscopy Test Conditions on the Results of Carbon Chemical Structure of Chars

Jiangyong He, Chong Zou *, Junxue Zhao *, Jiale Xi, Yuan She, Mengmeng Ren and Yufen Xu

School of Metallurgical Engineering, Xi'an University of Architecture and Technology, Xi'an 710311, China; hejiangyong55@126.com (J.H.); xjl610324@163.com (J.X.); sheyuan@xauat.edu.cn (Y.S.); ren.meng.meng@163.com (M.R.); xuyufen0612@163.com (Y.X.)

* Correspondence: zouchong@xauat.edu.cn (C.Z.); zhaojunxue1962@126.com (J.Z.)

Highlights:

- Uncertainty in the one-time measurement for chars by Raman spectroscopy technology is evident.
- Influence of char particle size and objective lens magnification on Raman characteristic parameters was investigated.
- The number of measurements required to obtain stable characteristic parameters is related to the micro-zone properties of the char surface.

Abstract: To address the problem of variability in in situ Raman spectroscopy for determining the chemical structure of chars, the rationality of Raman's original peak spectrum fitting method, the influence of objective lens magnification, particle size, and number of measurements on peak shape and characteristic parameters were investigated. The results show that the Raman original peak spectrum of char is fitted by five peaks and the goodness of fit is best when the D3 peak is fitted by a Gaussian curve. The intensity of the peak spectrum and stability of the characteristic parameters of the Raman spectroscopy are related to the objective lens magnification. For a relatively large objective lens magnification, the Raman peak spectrum intensity is increased and the coefficient of variation in the characteristic parameters is accordingly reduced. As particle size increases, the characteristic parameters A_G/A_{All} that characterize the perfect graphite structure decrease and the characteristic parameters A_{D1}/A_{All}, A_{D3}/A_{All}, and A_{D1}/A_G that characterize the defective graphite structure increase. The coefficient of variation for the characteristic parameters is found to be the smallest for the particle size range of 81–96 μm. Micro-Raman imaging reveals that the microscopic characteristic parameters of different micro zones are significantly different and the number of measurements required to achieve reliable Raman characteristic parameters is related to this anisotropy.

Keywords: Raman spectroscopy; coal pyrolysis; char; carbon chemical structure

check for updates

Citation: He, J.; Zou, C.; Zhao, J.; Xi, J.; She, Y.; Ren, M.; Xu, Y. Influence of Raman Spectroscopy Test Conditions on the Results of Carbon Chemical Structure of Chars. *Energies* **2022**, *15*, 5627. https://doi.org/10.3390/en15155627

Academic Editor: Rajender Gupta

Received: 5 July 2022
Accepted: 26 July 2022
Published: 3 August 2022

Publisher's Note: MDPI stays neutral with regard to jurisdictional claims in published maps and institutional affiliations.

Copyright: © 2022 by the authors. Licensee MDPI, Basel, Switzerland. This article is an open access article distributed under the terms and conditions of the Creative Commons Attribution (CC BY) license (https://creativecommons.org/licenses/by/4.0/).

1. Introduction

Raman spectroscopy is commonly used to characterize carbonaceous materials, such as coal and graphite, due to its wide applicability in the detection of crystals, molecules, and amorphous structures [1–4]. It also has the advantages of facile sample preparation, low minimum sample quantity, high resolution, high sensitivity, and being non-destructive. Therefore, it can provide reliable information for the evaluation of the orderliness of carbon chemical structures [5–9]. The half-width at maximum height, peak area ratio, peak position, and peak intensity of each peak obtained from the Raman peak fitting can be used to characterize the chemical structure of coal chars [5,10–14]. These characteristic parameters can also provide strong support for speculating on coal pyrolysis reaction surface adsorption mode, mechanical strength, and other properties [1,5,7,15].

Raman spectroscopy is widely used for analysis and research of coal char structure, precisely because this technique contains rich information characterizing coal char struc-

ture, although there have been a large number of studies with regard to utilization of Raman characteristic parameters to characterize the structure of coal chars. However, the Raman characteristic parameters selected to characterize the char structure are not always consistent [5,15–17]. For example, Sheng [5] selected the ratios between the peak spectrum intensities I_G/I_{All}, I_{D1}/I_G, and I_{D2}/I_G; Zou et al. [16] performed peak fitting of Raman spectra of coal chars and further processed peak areas (peak area ratios A_{D1}/A_G, A_G/A_{All}, and A_R/A_{All}) to construct the relationship between the coal char reaction performance and the ratios of Raman peak areas; Liu et al. [17] used Raman characteristic parameters, including peak spectral intensity, total peak area, peak position, and peak half-width at maximum height. On the other hand, the mode for testing conditions and the peak deconvolution method of the original Raman peak spectrum influence the conclusions that have been studied. Vidano et al. [18] studied the influence of four excitation wavelengths (488.0/514.5/568.2/647.1) on the Raman peak spectrum, where a progressive red-shift with increasing excitation wavelengths is evident for the D (1350 cm^{-1}) peak, whereas the positions of the G (1580 cm^{-1}) and D′ (1620 cm^{-1}) peaks are essentially invariant. Similar line-shift results were obtained for all of the samples investigated. Similarly, Sadezky et al. [19] and Matthews et al. [20] also arrived at the same conclusion. For the original Raman peak spectrum fitting research, Cuesta et al. [21] studied the Raman peak spectra of samples with different graphitization degrees and found that more comprehensive information of coal char could be obtained by multi-peak fitting of Raman original peak spectrum. Currently, the most commonly used method for coal char original peak spectrum fitting is five-peak fitting, including D4 peak at about 1150 cm^{-1}, D1 peak at about 1350 cm^{-1}, D3 peak at about 1530 cm^{-1}, G peak at about 1580 cm^{-1}, and D2 peak at about 1620 cm^{-1} [17,19,20]. However, there is no clear specification for the setting of objective lens magnification and coal char particle size. In particular, the objective lens magnification and particle size employed by different researchers to detect the microstructure of coal chars differs greatly. For example, the selected objective lens magnifications are 10× [22], 50× [17,23–25], and 100× [26], and particle sizes of coal chars are 48–96 [27], 74–105 [17], 105–150, and 150 μm [5], respectively. In addition, there are differences in Raman peak fitting methods for different carbonaceous materials. For example, it is more reasonable to adopt two-peak fitting for Raman peak spectrum of coke [28], while it is more reasonable to adopt five-peak fitting for some structure features of lignite and char, as they remain under cover around the D and G bands because of their disordered natures, although the five-peak fitting method of char Raman spectroscopy is generally accepted. However, there is controversy in the selection of fitting method for the D3 peak. Wang et al. [15] thought that Lorentz fitting was more reasonable, while Sadezky et al. [19] believed that Gaussian fitting was more reasonable. In addition, when Raman spectroscopy is applied to coal char structure detection and performance evaluation, the effects of variation in these testing conditions on characterizing coal char chemical structure have yet to be investigated.

In addition, some studies [29,30] have shown that the Raman characteristic parameters that characterize the coal char structure obtained after multiple Raman spectra of the same coal char sample exhibit variability. Taking A_{D1}/A_G as an example, the difference between the extrema of multiple detections can be as high as, approximately, three [29]. Rantitsch et al. used micro-Raman spectroscopy to measure and analyze the bulk cross-section of metallurgical coke with multiple data points. The standard deviations for the respective positions of the characteristic peak spectra from multiple measurements and the Raman characteristic parameters that characterize the structure differed, further demonstrating the non-uniformity of the metallurgical coke and the importance of multiple data points in the Raman spectroscopy detection process [30]. Unfortunately, the majority of studies adopted the results of one-time experimental analysis for Raman characteristic parameters to characterize the char structure. There are few studies on the influence of the number of spectra of a site on the stability of Raman characteristic parameters. Previous lab research suggested repeated Raman detection on a variety of char samples (particle size < 75 μm, excitation wavelength 514 nm, spectral resolution 1 cm^{-1}, objective lens magnification 20×)

and five-peak fitting. It is found that most of the Raman characteristic parameters of chars are quite different. Therefore, the accuracy of one-time Raman results predominantly used in studies of char structure analysis is questionable.

In this paper, the rationality of the two-peak deconvolution methods was evaluated by the value of goodness of fitting and a more reasonable fitting method for Raman peak spectrum was proposed. Subsequently, the influence of objective lens magnification and char particle size (<30, 61–75, 81–96, and 120–140 μm) on the intensity of the Raman peak spectrum, characteristic parameters, and their degree of stability are studied. As a result of the above, a method for obtaining average values (A_{D1}/A_G, A_G/A_{All}, A_{D3}/A_{All} and A_{D1}/A_{All}) through multiple Raman measurements is adopted to investigate the influence of the number of measurements on the stability of Raman characteristic parameters. Lastly, using micro-Raman imaging technology, a full scan of the micro zones of the char is performed to clarify the reasons for the differences in variability of the Raman characteristic parameters for different chars.

2. Experiment

2.1. Sample Preparation

Two coal chars (char1 and char2) were prepared from two industrial-scale pyrolyzers using low-rank coal obtained from northern Shaanxi, China. The pyrolysis temperature is controlled to be 600–750 °C, at a heating rate of 3–5 °C/min, and the pyrolysis time is 4–6 h. Before testing, the lump char was crushed, followed, and screened to the particle size intervals <30, 61–75, 81–96, and 120–140 μm, respectively. Then, the screened samples were dried at 105 °C for 2 h by drying in an oven. Proximate analysis of the samples is shown in Table 1.

Table 1. Proximate analysis of char1 and char2.

Sample	M_{ad}/%	A_{ad}/%	V_{ad}/%	FC_{ad}/%
Char1	0.93	7.57	12.38	79.12
Char2	1.21	8.45	7.38	82.96

ad: Air-dried basis.

2.2. Raman Spectroscopy Characterization

The Raman spectrometer (LabRAM ARAMIS, HORIBA Jobin Yvon Company, Paris, France) is employed to determine the carbon chemical structures in the samples. The infrared light excitation efficiency is low, the sensitivity is low, and the resonance effect of organic molecules is weak. Ultraviolet light has the characteristics of high energy and easy-to-damage samples. Both of them have obvious deficiencies in detecting coal char structure. However, the visible light with a wavelength of 514 nm has stable performance and can effectively detect the structure of organic molecules. Therefore, the selected Raman excitation wavelength is 514 nm. The Rayleigh scattering component was removed by a Notch filter and the Raman-scattered light was dispersed by an optical grid and detected by a CCD camera. The Raman spectrometer was generally operated in the continuous scanning mode. The exposure time was varied to find the optimum measurement conditions, and the exposure time mainly depends on the signal-to-noise ratio. In addition, spectral resolution is 1 cm^{-1} and the spectral scanning range is 500–2000 cm^{-1}. For the data obtained from Raman spectroscopy analysis, the data analysis and graphing software of origin is used for peak fitting by 5 peaks and the G, D1, D2, and D4 peaks are fitted in a Lorentzian manner; however, it needs to be further confirmed whether Gaussian or Lorentz fitting is adopted for D3 peak. Among those peaks, the G peak (about 1580 cm^{-1}) is an ideal graphitic lattice (E_{2g}-symmetry), representing the characteristic peak associated with a perfect graphite [6]. The larger the area of the G peak, the higher the degree of ordering of the chemical structure of coal coke. The D1 peak (about 1350 cm^{-1}) is commonly called the defect band (hereafter called D1 band), which corresponds to a graphitic lattice vibration mode with A_{1g} symmetry and is attributed to in-plane imperfections, such as defects

and heteroatoms [31]. The D2 peak (about 1620 cm^{-1}) always appears with the D1 peak and represents the stretching vibration of an irregular graphite lattice [32]. Its intensity decreases with the increase in the degree of organization. The D3 peak (about 1530 cm^{-1}) is related to the amorphous graphite, which is suggested to originate from the amorphous sp2-bonded forms of carbon, such as organic molecules, fragments, or functional groups, in poorly organized materials [21]. The D4 peak (about 1150 cm^{-1}) represents an irregular graphite structure and only appears in highly disordered materials [25]. The data resulting from peak fitting are further processed to obtain the quantitative Raman characteristic parameters that characterize the char microstructure.

To explore the effect of objective lens magnification on the obtained Raman characteristic parameters, char1 with a particle size of 61–75 μm is selected. Objective lens magnifications of 5×, 20×, and 50× are selected, resulting in corresponding laser beam diameters at the sample of 5.23 μm, 1.57 μm, and 0.84 μm, respectively. Observations corresponding to each objective lens magnification are repeated three times at the same site. The laser beam diameter corresponding to different objective lens multiples is calculated as shown in Equation (1).

$$D = 1.22\lambda/NA \quad (1)$$

where λ represents the excitation wavelength and NA represents the numerical aperture of the objective lens.

The effect of particle size on the Raman characteristic parameters is explored experimentally by changing the particle size with a fixed objective lens magnification of 20×. The four particle size intervals already described are used, and measurements corresponding to each particle size interval are repeated three times at the same site. To investigate the influence of the number of measurements on the stability of the results, char1 with objective lens magnification of 20× and a particle size of 61–75 μm is selected. Through multiple repeated sampling and measurements, stable Raman characteristic parameters are obtained and the obtained Raman characteristic parameters are further processed as follows: first, the standard deviation of the first two items is calculated and then differentiated, and the relation between the number of measurements and the stability of the Raman characteristic parameters is determined by the trend of the derivative of the standard deviation; meanwhile, in order to study the difference in the stability of the Raman characteristic parameters and the number of measurements of different samples, char2 is selected for comparison.

Micro-Raman imaging (HORIBA Jobin Yvon LabRam ARAMIS laser Raman spectrometer) is performed with a Raman imaging area of 30 μm × 50 μm to characterize the char structure. The selection of Raman excitation wavelength, spectral resolution, and spectral scanning range is consistent with that of conventional Raman detection and spatial resolution is 0.5 μm horizontally and 2 μm vertically.

3. Results and Discussion

3.1. Influence of Peak Deconvolution Method

Accurate fitting of the original Raman peak spectrum can obtain more accurate information for evaluating the structure of coal char. Figure 1 is the exemplary curve of using 4L1G (four Lorentz peaks and one Gaussian peak) and 5L (five Lorentz peaks) peak spectrum decomposing methods for Raman peak spectrum. It is impossible to evaluate the advantages and disadvantages of the two methods directly from Figure 1. Therefore, the data obtained by fitting are further compared. The rationality of the fitting method was evaluated by the χ^2/dof and it is generally believed that the smaller the value of χ^2/dof, the better the fitting effect. The goodness of fit achieved with the different peak combinations is indicated by the χ^2/dof values summarized in Table 2. When the original Raman peak spectrum is fitted by five peaks, regardless of the choice of objective lens multiple, the χ^2/dof of D3 peak by Gaussian fitting is smaller than that of the χ^2/dof of D3 peak by Lorentz fitting. The results show that from the perspective of goodness of fit, Gaussian fitting is more reasonable for the D3 peak. Similarly, other scholars [19] verified the rationality of Gaussian fitting for the D3 peak.

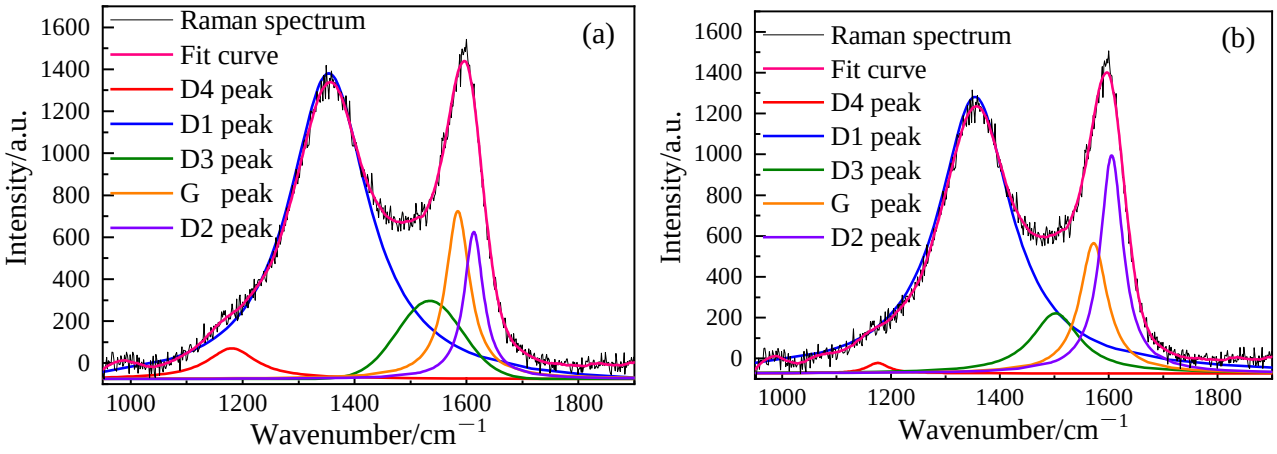

Figure 1. Raman original peak spectrum (objective lens magnification is 5×) five-peak fitting method; (**a**) 4L1G, (**b**) 5L.

Table 2. Goodness of fit for the Raman spectra of sample with different peak combinations (4L1G and 5L) and indicated by χ^2/dof value.

Times	Magnification/5×		Magnification/20×		Magnification/50×	
	4L1G/(χ^2/dof)	5L/(χ^2/dof)	4L1G/(χ^2/dof)	5L/(χ^2/dof)	4L1G/(χ^2/dof)	5L/(χ^2/dof)
1	1.02	1.12	0.82	1.62	1.84	3.41
2	0.85	2.30	0.76	1.36	1.20	2.70
3	0.70	2.04	1.10	1.51	3.57	4.56

χ^2/dof: Chi-square/degree of freedom.

Figure 2 shows that the peak position and area ratio of each peak by using different fitting methods. As can be seen from Figure 2a, compared with the 5L fitting method, the position of G, D2, and D3 peaks shift to higher wavenumbers; among them, the peak shift of the D3 peak is the most obvious, whereas the D1 and D4 peak have no obvious change trend when 4L1G fitting is used. Then, the difference in peak position is further analyzed in detail, and the peak position of D3, G, D2, and D4 increase from 1503.47 to 1531.73 cm^{-1}, 1571.36 to 1578.70 cm^{-1}, 1601.73 to 1606.63 cm^{-1}, and 1178.43 to 1180.34 cm^{-1}. Obviously, the peak position of the D3 peak was the most varied. In addition, the peak area ratio of the characteristic structure in Figure 2b is analyzed. The value of A_G/A_{All} and A_{D2}/A_{All} obtained by 4L1G fitting is 12.21% and 8.73%, which is less than that obtained by 5L fitting. On the contrary, the values of A_{D1}/A_{All}, A_{D3}/A_{All} and A_{D4}/A_{All} obtained by 4L1G fitting are greater than those obtained by 5L fitting. This phenomenon indicates that the shift in the peak position will cause the ratio of the spectral area of each peak to show a difference and then make the evaluation of char structure show the difference (the order of the structure of the char obtained by the 4L1G fitting method is lower than that of the 5L fitting method). Previous studies [27] have shown that the peak movement is mainly due to structural changes; the peak positions of D1, D2, and D3 shift to lower wavenumber due to the fracture of the heteroatom groups, functional groups, and smaller aromatic ring systems, which can easily be attacked by hydrogen. The G peak position shifts toward higher wavenumbers, which might be caused by destruction of the organic molecule fragments. In addition, the shift of peak position will lead to a change in peak spectral area and peak spectral area is an important parameter to characterize the degree of ordering of coal coke. For example, it is generally considered that the area of the G peak is positively correlated with the degree of ordering of coal char. A series of conclusions shows that the position of the peak is very important for evaluating the structure of char.

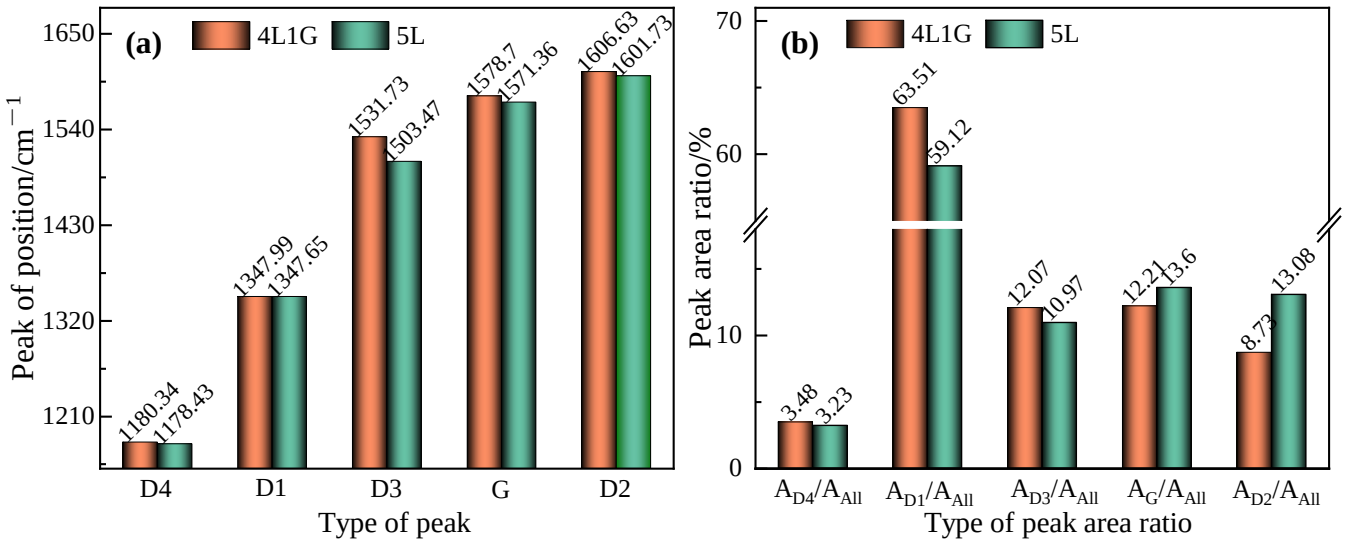

Figure 2. Peak positions (**a**) and peak area ratios (**b**) obtained by different fitting methods.

Due to the complexity of the chemical structure of char, it is impossible to evaluate the pros and cons of the two fitting methods through the peak position and peak area ratio. However, an obvious phenomenon was found that the Raman parameters are different when obtained by different fitting methods. This will affect the prediction of the char properties (reactivity, grindability, strength . . .). There is a large number of studies [5,10,12–15] showing that the Raman parameters are important parameters for characterizing char structure and further predicting char properties. This phenomenon indicates that the characterization of char structure by Raman spectroscopy needs further research.

Although the best fitting method cannot be determined by peak shape, peak position, and peak area ratio, the fitting method of 4L1G is considered to be more reasonable based on the goodness of fit. Therefore, the fitting method of 4L1G is adopted for all the Raman peak spectra in this paper.

3.2. Influence of Magnification of Objective Lens

Figure 3 demonstrates the intensity variation in the Raman peak spectra obtained from three observations for each respective objective lens magnification for char1. It can be clearly seen that the intensity of the Raman peak spectra of char1 varies with objective lens magnification. When the objective lens magnification increases, the Raman peak spectrum intensity gradually increases. The intensity of the Raman peak spectrum is mainly affected by the Raman scattering power, absorbance, aromatic ring size, and oxygen-containing functional groups in the sample [14,25]. For the same char, differences in the peak spectrum intensity for different objective lens magnifications are mainly due to the fact that as the objective lens magnification increases, the corresponding numerical aperture increases. Under the conditions of the same excitation laser energy and probability of Raman scattering, the larger the numerical aperture, the larger the number of photons scattered, which leads to increased Raman scattering. This increased Raman scattering is conducive to improving the spatial resolution. Further, the solid angle of Raman scattering signal collection in the Raman spectrum detection process is increased.

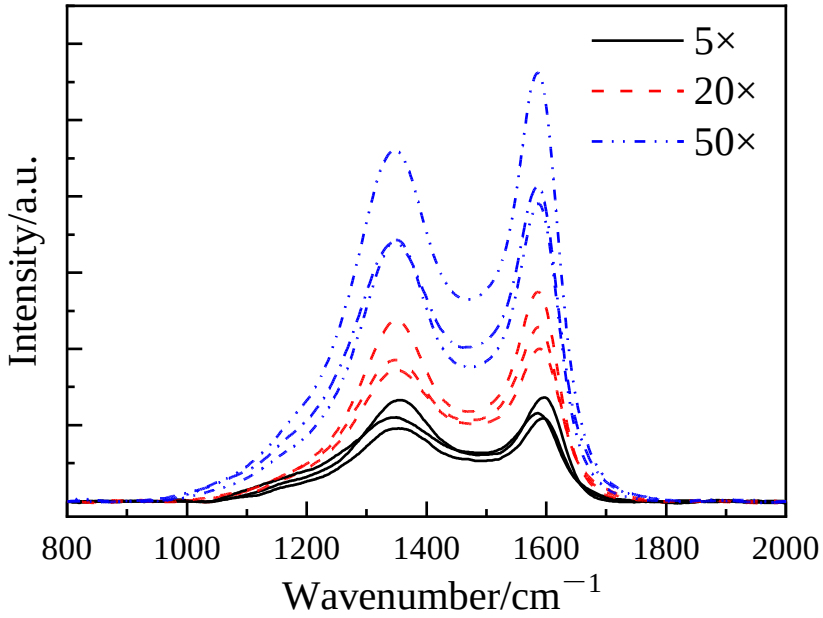

Figure 3. Raman peak intensity for char1 with a particle size of 61–75 μm for different objective lens magnifications.

Figure 4 presents the Raman characteristic parameters of char1 for different objective lens magnifications. It can be seen from Figure 4 that as the objective lens magnification increases, the Raman characteristic parameters A_{D1}/A_{All} and A_{D1}/A_G show a decreasing trend, whereas A_G/A_{All} and A_{D3}/A_{All} show an increasing trend. Although the Raman characteristic parameters reflect a certain variation mechanism, the difference is relatively small. However, there is an obvious phenomenon that can be observed: the stability of Raman characteristic parameters corresponding to different objective lens magnifications is quite different. When the objective lens magnification is higher, the stability of the Raman characteristic parameters is increased. A possible reason for this phenomenon is as follows: when the objective lens magnification is lower, the diameter of the corresponding laser beam is larger and there are more particles included in the beam diameter. Since the microstructure of the char main body is a heterogeneous high polymer that is highly cross-linked in three-dimensional space, the crystal structures of different particles are quite different. Therefore, the characteristic parameters have a relatively large variability in Raman spectroscopy analysis and detection.

The Raman characteristic parameters of char1 under different objective lens magnifications and the coefficients of variation that characterize the stability of the parameters are listed in Table 3. It can be seen from Table 3 that as the objective lens magnification increases, the variation coefficients of all the Raman characteristic parameters exhibit a downward trend; when the objective lens magnification is 50×, the corresponding variation coefficients are significantly smaller than the variation coefficients corresponding to the objective lens magnifications of 5× and 20×. Taking the coefficient of variation corresponding to the characteristic parameter A_{D1}/A_{All} as an example, the values corresponding to the 5× and 20× objective lenses are 0.044 and 0.017, respectively, whereas the value corresponding to the 50× objective lens is only 0.002.

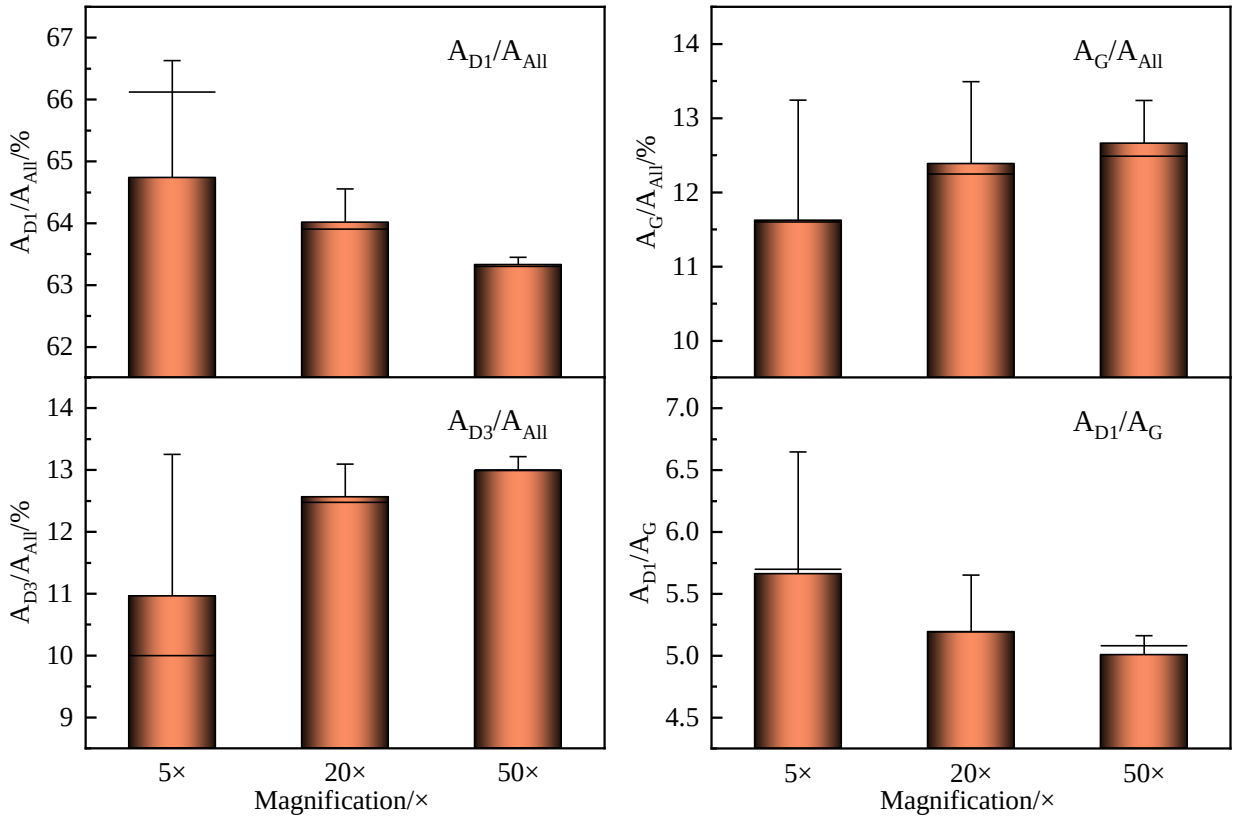

Figure 4. Raman characteristic parameters of char1 with a particle size of 61–75 μm for different objective lens magnifications.

Table 3. Variation coefficients of Raman characteristic parameters of char1 under different lens magnifications.

Magnification/×	Coefficient of Variation			
	A_{D1}/A_{All}/%	A_G/A_{All}/%	A_{D3}/A_{All}/%	A_{D1}/A_G
5	0.044	0.139	0.182	0.177
20	0.017	0.085	0.071	0.101
50	0.002	0.040	0.018	0.042

The coefficient of variation characterizes the degree of dispersion in the data.

The magnitude of the coefficient of variation characterizes the degree of dispersion in the data; when the value is relatively large, a greater degree of variation in the data is indicated, while a smaller value indicates a smaller degree of variation. In terms of the results of this study, the degree of dispersion in the Raman characteristic parameters obtained with a 50× objective lens are the smallest. This result suggests that choosing a high-spatial-resolution objective lens is conductive to the enhancement of the stability of Raman characteristic parameters.

3.3. Influence of Particle Size of Samples

The intensity differences in the Raman peak spectrum corresponding to four different particle sizes of char1 are displayed in Figure 5. As can be seen from Figure 5, there is no correlation between the intensity of the original Raman peak spectrum and the particle size of char.

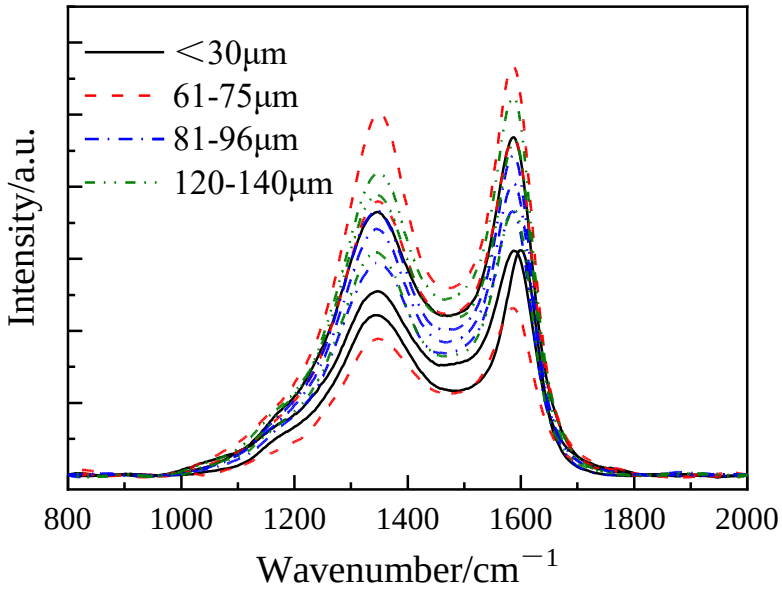

Figure 5. Raman peak spectrum intensity of char1 for different particle sizes.

However, there is an obvious phenomenon that can be observed in Figure 5. The FWHM of the D peak characterizing char1 carbon atom lattice defects is greater than the G peak characterizing the ideal graphite lattice structure. This is mainly because char is a medium- to low-temperature pyrolysis solid product and the promotion effect of pyrolysis on the degree of coalification is limited. In chars, there are numerous aliphatic, alicyclic, and lateral chain small molecular structures that characterize lattice structure defects. After referring to the proximate analysis in Table 1, it can be seen that the volatile content of char1 reaches 12.38%. Some studies [33,34] show that with increasing volatile content in chars, the degree of coalification decreases and there are more amorphous carbons and disordered graphite lattice structures characterizing graphite defect structures in chars; in addition, the FWHM difference between the D and G peaks is also used to characterize the ordering degree of chars. The higher the degree of coalification, the smaller the FWHM difference between the D and G peaks [35]. The results are consistent with the results of this work.

Figure 6 shows the variation in typical Raman characteristic parameters corresponding to char1 for different particle sizes. It can be seen from Figure 6 that as the particle size of the char increases, the Raman characteristic parameters A_{D1}/A_{All}, A_{D3}/A_{All}, and A_{D1}/A_G that characterize the defect structures of the chars all increase and the Raman characteristic parameter A_G/A_{All} that characterizes the perfect graphite structure of the chars decreases. This phenomenon indicates that under the same testing conditions, an increase in particle size will increase the parameters that characterize the defect structures of chars. Char itself is an intricate heterogeneous substance composed of defective graphite structure, amorphous carbon structure, and perfect graphite structure. As char is a solid product of bituminous coal after medium- and low-temperature pyrolysis, the degree of coalification is relatively low. This leads to the phenomenon where perfect graphite structures, which are a smaller proportion of the chars, which characterize the high degree of coalification, are more extensively wrapped by the defective graphite structures. Thus, a large number of perfect graphite structures is exposed during the char grinding process. Therefore, the smaller the particle size, the greater the A_G/A_{All} ratio, and the smaller the Raman characteristic parameters that characterize the defective graphite structures.

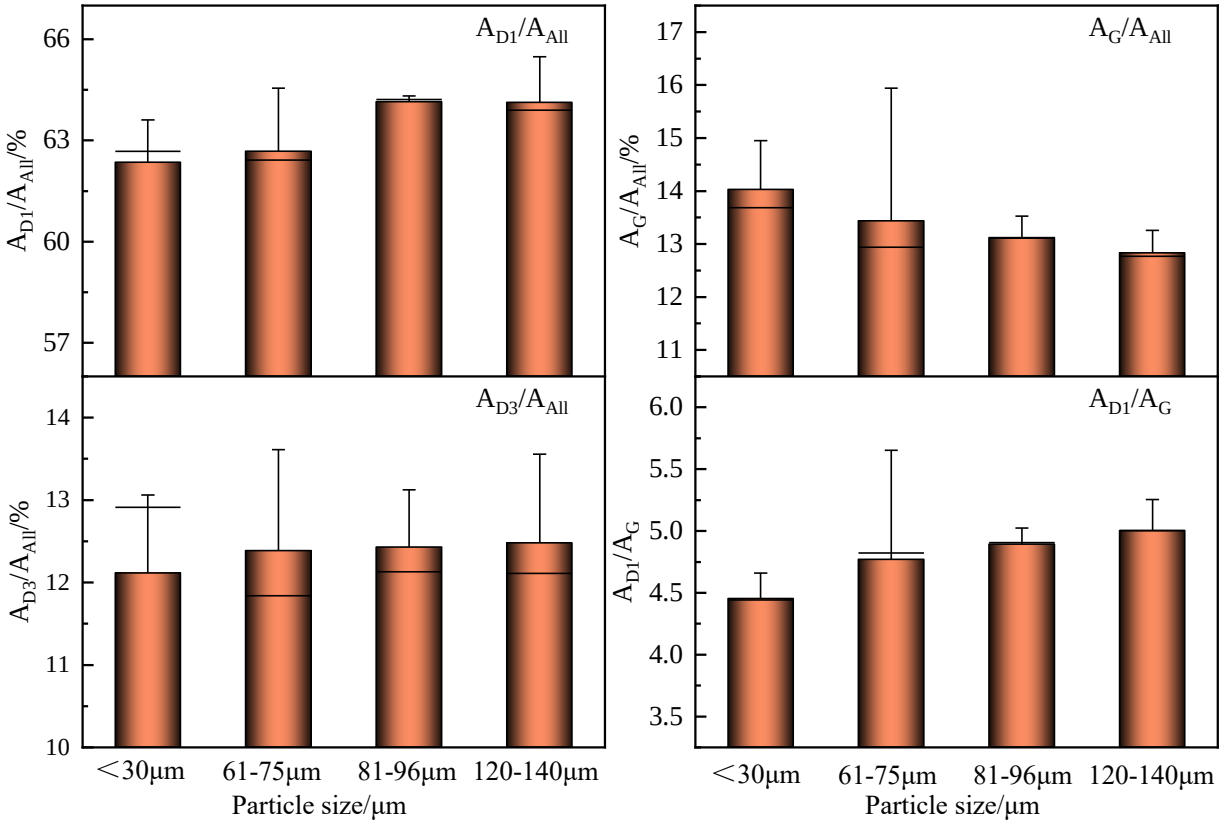

Figure 6. Raman characteristic parameters of char1 for different particle sizes.

Table 4 lists the Raman characteristic parameters of char1 for different particle sizes and the coefficients of variation that characterize the stability of the Raman characteristic parameters. In terms of the average value of the Raman characteristic parameters, the average values of the particle size intervals of <30 and 61–75 μm are relatively close, as are those of 81–96 μm and 120–140 μm. Taking A_{D1}/A_{All} as an example, the values of the particle size intervals of <30 and 61–75 μm are 62.35% and 62.67%, respectively, and the values of 81–96 μm and 120–140 μm are 64.14% and 64.13%, respectively.

Table 4. Coefficient of variation in Raman characteristic parameters for different particle sizes of char1.

Particle Size	Coefficient of Variation			
	A_{D1}/A_{All}/%	A_G/A_{All}/%	A_{D3}/A_{All}/%	A_{D1}/A_G
<30 μm	0.023	0.058	0.125	0.045
61–75 μm	0.028	0.171	0.085	0.191
81–96 μm	0.003	0.031	0.048	0.028
120–140 μm	0.019	0.031	0.076	0.050

Additionally, the coefficients of variation corresponding to the Raman characteristic parameters are further quantitatively analyzed and compared. The coefficients of variation corresponding to the Raman characteristic parameters of char1 for different particle sizes exhibit large differences. The coefficients of variation corresponding to the different Raman characteristic parameters for a particle size of 81–96 μm are the smallest for all peaks; the coefficients of variation corresponding to the Raman characteristic parameters with particle sizes of <30 and 61–75 μm are close and are significantly larger than the coefficients of variation corresponding to the Raman characteristic parameters with particle size intervals of 81–96 μm and 120–140 μm. This indicates that, for this study, the Raman characteristic

parameters obtained by selecting the chars with a particle size interval of 81–96 μm are of better stability. Based on the further analysis of the variation in Raman characteristic parameters with particle size, a possible reason for this phenomenon is that when char1 has a particle size interval of 81–96 μm, the uniformity of characterizing the char defects and perfect graphite structure composition is superior.

According to the comparison of the effects for the char particle size and the objective lens magnification on the Raman characteristic parameters in the above two sections, it is concluded that changing the particle size and objective lens magnification will cause the Raman characteristic parameters to show a certain regular variation trend. However, the differences between the Raman characteristic parameters for different conditions are small. Taking the Raman characteristic parameter A_{D1}/A_{All} as an example, the difference between extreme values for different objective lens magnifications and particle sizes are only 1.41% and 1.79%, respectively. A possible reason for the differences is that the char itself is composed of heterogeneous units and that components are segregated. Nevertheless, from the perspective of the variability in Raman characteristic parameters for different conditions, there are large differences for the two conditions. Referring to Tables 3 and 4, it can be seen that when the objective lens magnification is 50×, the corresponding laser beam diameter is 0.84 μm, and for a particle size of 81–96 μm, the coefficient of variation is the smallest. This result reflects the importance of selecting the appropriate beam diameter (objective lens) and particle size to increase the stability of the results of Raman spectroscopy.

3.4. The Influence of the Number of Measurements on the Stability of the Results

Table 5 lists typical Raman characteristic parameters of char 1 and char 2 with particle sizes of 61–75 μm after multiple Raman analyses of the same site. It can be observed from Table 5 that there are significant differences in the results of some Raman experiments. Taking the A_G/A_{All} as an example, the extreme value difference of char1 reaches about 6%; while that of char 2 is about 15%. Experimental results with large variability will affect the evaluation of the microstructures of the chars and, thus, the predicted properties of the chars. However, the relationship between the stability of the characteristic parameters and the number of measurements cannot be directly achieved by the Raman characteristic parameters from multiple measurements alone. Thus, further data processing should be performed on the obtained Raman characteristic parameters.

In Figure 7, the variation trend for the standard deviation and derivative of the Raman characteristic parameters of char1 for a particle size of 61–75 μm, as the number of measurements increases, is shown. It can be seen from Figure 7 that as the number of measurements increases, all standard deviations decrease, and the corresponding derivatives gradually stabilize. The phenomenon indicates that the method of obtaining the mean value by repeated measurement can improve the stability of the obtained results. For the selected Raman characteristic parameters A_{D1}/A_G, A_{D1}/A_{All}, A_{D3}/A_{All}, and A_G/A_{All}, the derivatives of the standard deviations, which characterize the stability of Raman characteristic parameters, vary greatly in the first five measurements. The ranges of variation become narrower until the eighth experiment. The slopes corresponding to the standard deviations reach a relatively stable state, which indicates that relatively stable Raman characteristic parameter values can be achieved by taking the average value of char1 by eight successive Raman observation analyses.

Table 5. Characteristic parameters obtained from multiple Raman measurements for char1 and char2 with a particle size of 61–75 μm.

Times	Char1						Char2					
	A_{D4}/A_{All}/%	A_{D1}/A_{All}/%	A_{D3}/A_{All}/%	A_G/A_{All}/%	A_{D2}/A_{All}/%	A_{D1}/A_G	A_{D4}/A_{All}/%	A_{D1}/A_{All}/%	A_{D3}/A_{All}/%	A_G/A_{All}/%	A_{D2}/A_{All}/%	A_{D1}/A_G
1	6.78	55.69	13.32	14.47	9.73	3.85	3.12	68.50	8.72	13.05	6.61	5.25
2	5.68	67.67	10.01	9.97	6.67	6.79	8.75	45.20	10.93	25.36	9.77	1.78
3	0.70	64.06	13.44	12.57	9.23	5.09	8.71	49.65	10.87	17.57	13.20	2.82
4	0.86	61.05	11.71	15.94	10.44	3.83	4.53	63.55	9.15	15.95	6.83	3.98
5	3.78	62.41	11.84	12.94	9.02	4.82	12.40	46.00	11.55	16.50	13.55	2.79
6	1.05	64.55	13.61	11.42	9.36	5.65	2.95	48.24	22.34	21.97	4.51	2.20
7	1.39	63.91	12.48	13.49	8.73	4.74	6.30	50.13	7.61	28.90	7.06	1.73
8	0.84	63.59	13.81	12.25	9.52	5.19	1.36	69.30	6.58	18.21	4.54	3.80
9	2.05	63.10	13.14	12.91	8.79	4.89	11.03	37.61	14.13	28.16	9.08	1.34
10	4.07	62.62	13.00	11.86	8.46	5.28	3.58	67.04	4.67	18.53	6.18	3.62
11	0.97	64.31	12.91	12.82	8.98	5.02	8.56	48.77	12.73	18.29	11.66	2.67
12	4.85	62.30	11.75	12.79	8.31	4.87	1.35	62.73	9.02	18.58	8.31	3.38
13	-	-	-	-	-	-	5.22	56.12	8.70	17.95	12.02	3.13
14	-	-	-	-	-	-	7.45	54.15	9.99	17.25	11.16	3.14
15	-	-	-	-	-	-	5.28	55.76	8.38	20.27	10.31	2.75

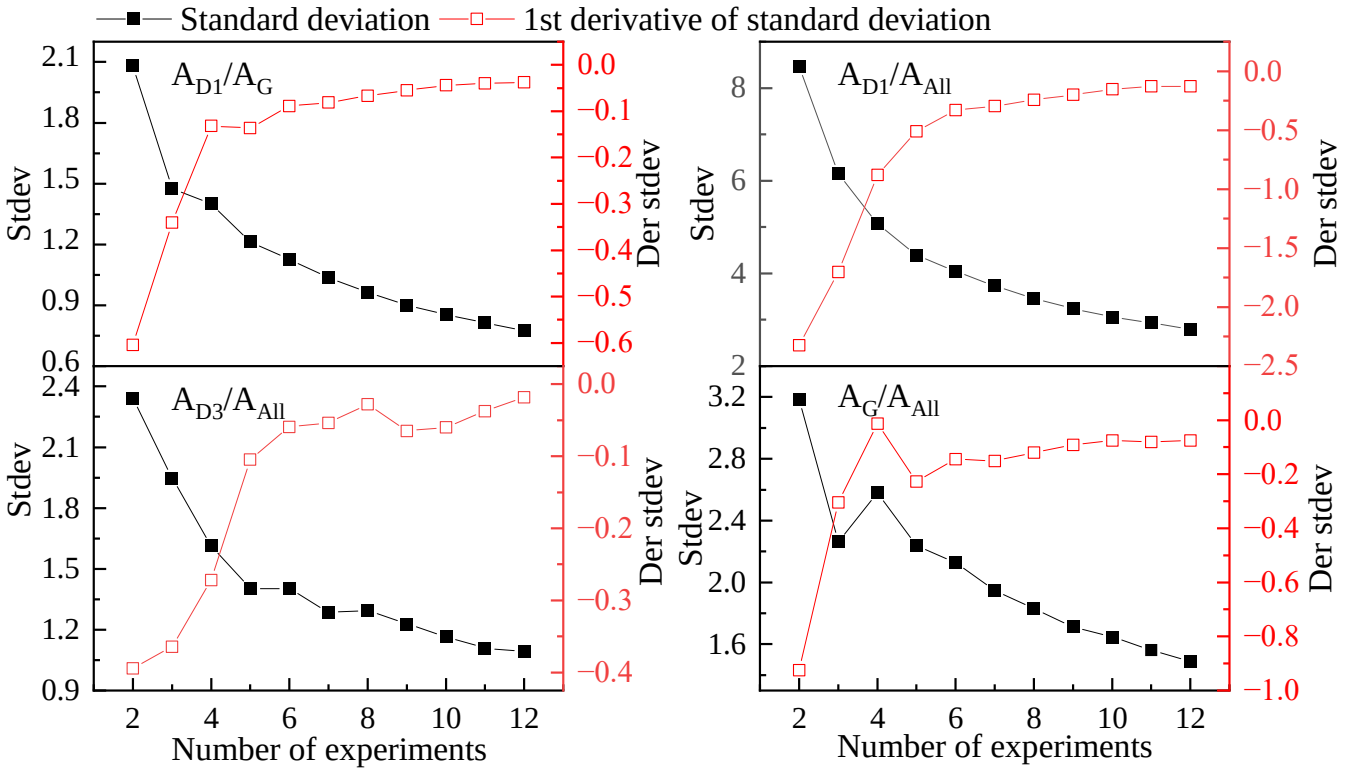

Figure 7. Standard deviations and corresponding derivatives of char1 Raman characteristic parameters.

Figure 8 presents the variation trend for the standard deviations corresponding to the Raman characteristic parameters and the derivatives corresponding to the standard deviations of the contrasting sample char 2, with an increased number of Raman measurements. In contrast to the variation trend shown in Figure 7, it can be seen that the standard deviation and derivative trends corresponding to the Raman characteristic parameters of char 2 are more complicated. For example, the mean values of the characteristic parameters A_{D1}/A_{All} and A_G/A_{All} do not exhibit a one-fold variation trend with an increasing number of measurements. Moreover, there are differences between the number of measurements required for the derivatives corresponding to the standard deviations of different Raman characteristic parameters to stabilize. Although the variation trend is relatively complicated, there are still some similarities with char1. As the number of measurements increases, the derivatives corresponding to the standard deviations in the Raman characteristic parameters tend to stabilize. For instance, after eight measurements, the derivatives corresponding to the standard deviations of A_{D1}/A_G and A_{D3}/A_{All} become stable, whereas the derivatives of the standard deviations of A_{D1}/A_{All} and A_G/A_{All} do not stabilize until after ten Raman measurements.

In order to further clarify the difference in the fluctuation of the two chars' Raman characteristic parameters, the coefficients of variation for the characteristic parameters of the two chars are calculated for later comparison. Table 6 shows the coefficients of variation corresponding to the characteristic parameters of the two chars. By comparing the variation mechanisms of the coefficients of variation in Table 6, it can be found that as the number of measurements increases, the coefficients of variation corresponding to the Raman characteristic parameters of the two chars gradually decrease and become stable. Under the same conditions, by comparing the differences between the coefficients of variation for the two chars, it can be seen that the coefficients of variation for char1 are smaller than those for char2, which may be because the char is a three-dimensional highly cross-linked heterogeneous high polymer polycondensate, composed of numerous heterogeneous basic structural units whose microscopic molecular structure is extremely complex, thereby leading to the phenomenon that the variability in different chars is

quite different during the Raman detection process. In order to verify the existence of the difference in the uniformity of the microstructural composition of these chars, further discussion is presented in Section 3.5.

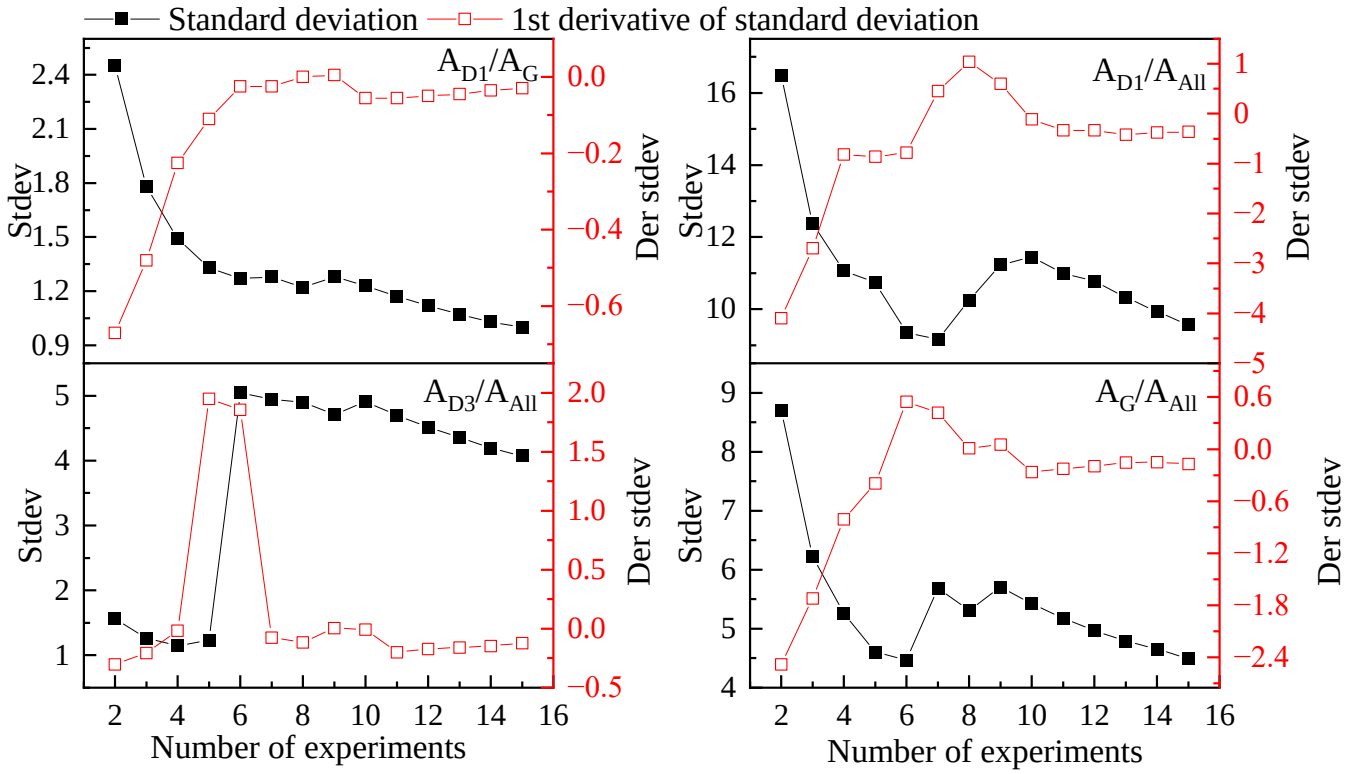

Figure 8. Standard deviations and corresponding derivatives of char2 Raman characteristic parameters.

Table 6. Variation coefficients of Raman parameters for char1 and char2 for different detection times.

Times	Char1 of Coefficient of Variation				Char2 of Coefficient of Variation			
	A_{D1}/A_{All}/%	A_G/A_{All}/%	A_{D3}/A_{All}/%	A_{D1}/A_G	A_{D1}/A_{All}/%	A_G/A_{All}/%	A_{D3}/A_{All}/%	A_{D1}/A_G
2	0.140	0.260	0.201	0.39	0.29	0.45	0.16	0.70
3	0.098	0.183	0.159	0.282	0.23	0.33	0.12	0.54
4	0.082	0.195	0.133	0.286	0.20	0.29	0.12	0.43
5	0.071	0.170	0.116	0.248	0.20	0.26	0.12	0.40
6	0.065	0.165	0.114	0.225	0.17	0.24	0.41	0.40
7	0.059	0.201	0.104	0.208	0.17	0.29	0.43	0.44
8	0.055	0.142	0.103	0.193	0.19	0.27	0.45	0.40
9	0.052	0.133	0.098	0.181	0.21	0.28	0.42	0.45
10	0.049	0.129	0.092	0.171	0.21	0.27	0.46	0.42
11	0.047	0.122	0.088	0.162	0.20	0.26	0.43	0.40
12	0.044	0.116	0.087	0.155	0.20	0.25	0.42	0.38
13	-	-	-	-	0.19	0.24	0.41	0.36
14	-	-	-	-	0.18	0.24	0.40	0.35
15	-	-	-	-	0.17	0.23	0.39	0.34

3.5. Analysis of the Cause of Variability in Raman Results

Figure 9 presents the 30 μm × 50 μm scan of local areas of char1 and char2, with a particle size of 61–75 μm, using Raman microscopy. The contour maps of the two main characteristic parameters A_G/A_{All} and A_{D1}/A_{All} are plotted by the peak fitting processing of a large amount of raw Raman data. According to the differences between the color transitions in the characteristic parameters and some of the main parameter values shown in Figure 9, it can be seen that there are large differences between the characteristic parameters

A_G/A_{All} and A_{D1}/A_{All} in the chars in the selected zone of 30 μm × 50 μm; the span interval of Raman characteristic parameter contour value is large. For example, the span range of A_G/A_{All} contour values of char1 and char2 is 7.46–21.7% and 4.63–21.7%, respectively. The span interval of the A_{D1}/A_{All} contour value was 48.0–65.3% and 30.8–65.5%, respectively. This phenomenon verifies the complexity and heterogeneity of the micro-crystal structure of chars and also indicates that when using Raman spectroscopy to characterize the chemical structure of chars, there is a large uncertainty in the chemical structure determined through a small number of measurements. Since the micro-carbon chemical structure of chars is an important indicator to characterize the physical and chemical properties, it plays an important guiding role in the prediction of char performance and the terminal utilization approaches and utilization methods of chars. Therefore, when the carbon chemical structure is characterized by the Raman characteristic parameters, particular attention should be paid to the complexity and particularity of the char structure and whether the selected Raman characteristic parameters are representative of the chemical structure of the char.

Using Figure 9 for further analysis, the A_G/A_{All} and A_{D1}/A_{All} contour lines of char1 are less dense than those of char2, which indicates better uniformity in the micro-carbon chemical structure. Therefore, char1 is shown to require fewer Raman measurements to obtain stable Raman characteristic parameters that characterize the char structure; under the condition of the same number of Raman measurements, the coefficients of variation of char1 characterizing the stability of Raman characteristic parameters are always smaller than those of char2. As observed, the number of measurements required to obtain stable Raman characteristic parameters is related to the anisotropy of the micro-zone properties at the char surface.

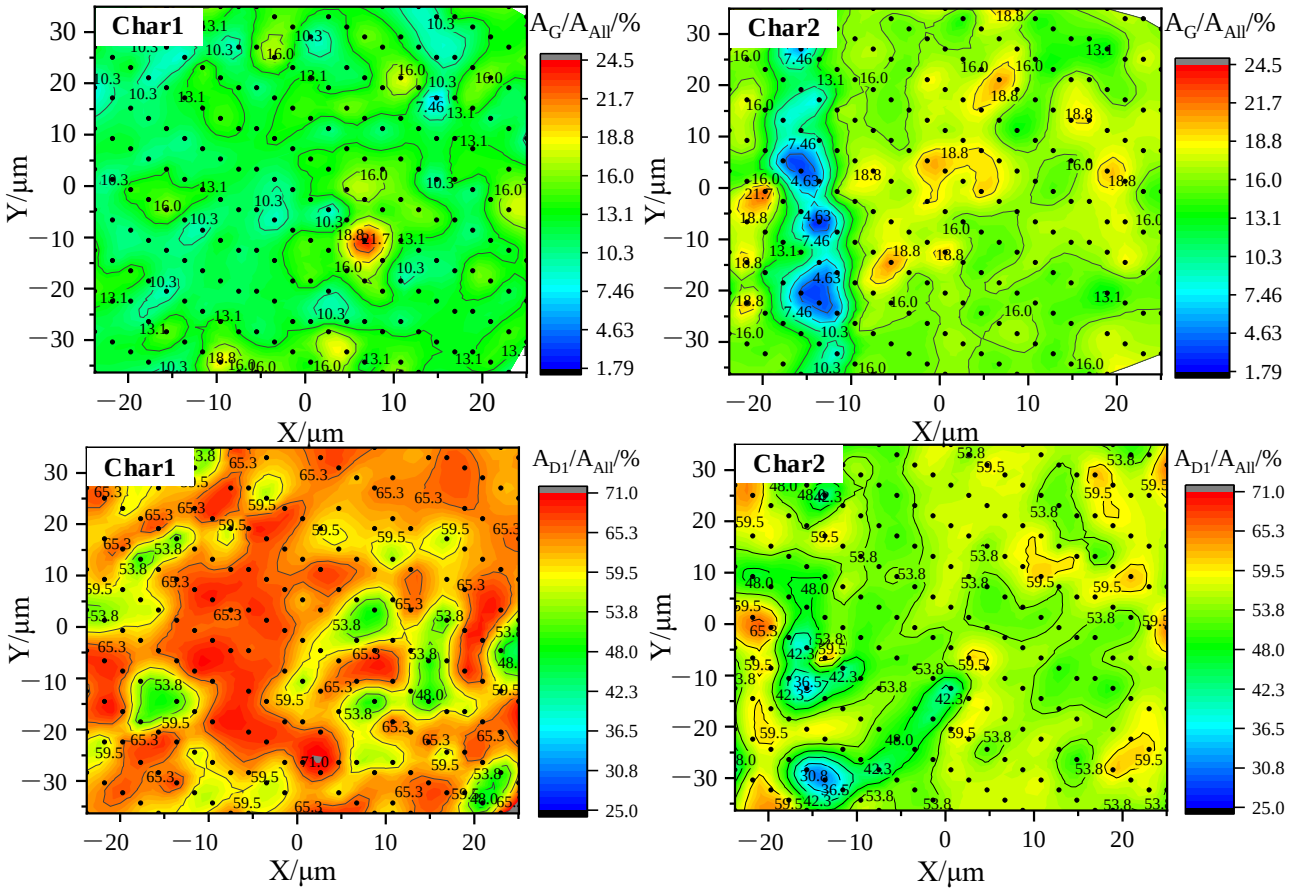

Figure 9. Two-dimensional contour maps of the characteristic parameters A_G/A_{All} and A_{D1}/A_{All} of char1 and char2.

4. Conclusions

1. As far as goodness of fit is concerned, it is more reasonable to adopt Gaussian fitting for the D3 peak of char Raman spectrum. Compared with Lorentz fitting, Gaussian fitting makes the positions of D3 and G peaks shift to the right and the D3 peak position changed more obviously. In addition, A_{D1}/A_{All}, A_{D3}/A_{All}, and A_{D4}/A_{All} increased while A_G/A_{All} and A_{D2}/A_{All} decreased.
2. The objective lens magnification affects the intensity of the Raman peak spectrum. The greater the objective lens magnification, the higher the intensity of the Raman peak spectrum. In addition, when the objective lens magnification is 50×, the coefficient of variation that characterizes the stability of the Raman parameter is the smallest.
3. There is no correlation between the intensity of the original Raman peak spectrum and the particle size. A_{D1}/A_G, A_{D1}/A_{All}, and A_{D3}/A_{All}, which characterize the defect structures of char, gradually increase with increasing particle size; however, the characteristic parameter A_G/A_{All}, which characterizes the perfect graphite structure of chars, decreases with an increase in particle size.
4. The number of measurements required to obtain stable Raman characteristic parameters of chars is related to the micro-zone properties of the char surface. The higher the degree of uniformity in the carbon structure of the char micro-zones, the lower the number of measurements required and the smaller the coefficients of variation.

Author Contributions: J.H.: Writing—original draft, Investigation; C.Z.: Formal analysis, Methodology; J.Z.: Formal analysis; J.X.: Writing—Review and Editing; Y.S.: Supervision; M.R.: Supervision; Y.X.: Writing—Review and Editing. All authors have read and agreed to the published version of the manuscript.

Funding: Key Research and Development Program of Shannxi (2021GY-128, 2020GY-229).

Institutional Review Board Statement: Not applicable.

Informed Consent Statement: Not applicable.

Data Availability Statement: The data that support the findings of this study are available from the corresponding author, [Chong Zou], upon reasonable request.

Conflicts of Interest: The authors declare that they have no known competing financial interest or personal relationships that could have appeared to influence the work reported in this paper.

References

1. Quirico, E.; Rouzaud, J.; Bonal, L.; Montagnac, G. Maturation grade of coals as revealed by Raman spectroscopy: Progress and problems. *Spectrochim. Acta Part A* **2005**, *61*, 2368–2377. [CrossRef] [PubMed]
2. Li, X.; Hayashi, J.; Li, C. FT-Raman spectroscopic study of the evolution of char structure during the pyrolysis of a Victorian brown coal. *Fuel* **2006**, *85*, 1700–1707. [CrossRef]
3. Hinrichs, R.; Brown, M.; Vasconcellos, M.T.; Abrashev, M.V.; Kalkreuth, W. Simple procedure for an estimation of the coal rank using micro-Raman spectroscopy. *Int. J. Coal Geol.* **2014**, *136*, 52–58. [CrossRef]
4. Zhang, X.; Zhang, C.; Tan, P.; Li, X.; Fang, Q.; Chen, G. Effects of hydrothermal upgrading on the physicochemical structure and gasification characteristics of Zhundong coal. *Fuel Process. Technol.* **2018**, *172*, 200–208. [CrossRef]
5. Sheng, C. Char structure characterised by Raman spectroscopy and its correlations with combustion reactivity. *Fuel* **2007**, *86*, 2316–2324. [CrossRef]
6. Tuinstra, F.; Koenig, J.L. Raman Spectrum of Graphite. *J. Chem. Phys.* **1970**, *53*, 1126–1130. [CrossRef]
7. Green, P.D.; Johnson, C.A.; Thomas, K. Applications of laser Raman microprobe spectroscopy to the characterization of coals and cokes. *Fuel* **1983**, *62*, 1013–1023. [CrossRef]
8. Wang, X.; Gong, Y.; Wang, X.; Jin, B. Experimental and kinetics investigations of separated-gasification chemical looping combustion of char with an iron ore as the oxygen carrier. *Fuel Process. Technol.* **2020**, *210*, 106554. [CrossRef]
9. Knight, D.S.; White, W.B. Characterization of diamond films by Raman spectroscopy. *J. Mater. Res.* **1989**, *4*, 385–393. [CrossRef]
10. Ma, C.; Zou, C.; Zhao, J.; Shi, R.; Li, X.; He, J.; Zhang, X. Pyrolysis Characteristics of Low-Rank Coal under a CO-Containing Atmosphere and Properties of the Prepared Coal Chars. *Energy Fuel* **2019**, *33*, 6098–6112. [CrossRef]
11. Yoshida, A.; Kaburagi, Y.; Hishiyama, Y. Full width at half maximum intensity of the G band in the first order Raman spectrum of carbon material as a parameter for graphitization. *Carbon* **2006**, *44*, 2330–2356. [CrossRef]

12. Zaida, A.; Bar-Ziv, E.; Radovic, L.; Lee, Y. Further development of Raman Microprobe spectroscopy for characterization of char reactivity. *Proc. Combust. Inst.* **2007**, *31*, 1881–1887. [CrossRef]
13. Liu, L.; Kong, B.; Yang, J.; Liu, Q.; Liu, X. CO_2 Gasification Kinetics and Structural Characteristics of Tri-High Coal Char Prepared at Elevated Temperature. *Am. Chem. Soc.* **2020**, *5*, 507–517. [CrossRef] [PubMed]
14. Li, M.; Zeng, F.; Qi, F.; Sun, B. Raman Spectroscopic Characteristics of Different Rank Coals and the Relation with XRD Structural Parameters. *Spectrosc. Spectr. Anal.* **2009**, *29*, 2446–2449.
15. Wang, B.; Sun, L.; Su, S.; Xiang, J.; Hu, S.; Fei, H. Char Structural Evolution during Pyrolysis and Its Influence on Combustion Reactivity in Air and Oxy-Fuel Conditions. *Energy Fuel* **2012**, *26*, 1565–1574. [CrossRef]
16. Zou, C.; He, J.; Zhao, J.; Li, X.; Shi, R.; Ma, C.; Kang, Y.; Zhang, X. Structure and Reactivity of Low-Rank Coal Chars Prepared from Fluidized Bed and Moving Bed Pyrolyzers and the Potential for Using Them in Pulverized Coal Injection (PCI). *Met. Mater. Trans. A* **2019**, *50*, 2304–2318. [CrossRef]
17. Xu, J.; Tang, H.; Su, S.; Liu, J.; Xu, K.; Qian, K.; Wang, Y.; Zhou, Y.; Hu, S.; Zhang, A.; et al. A study of the relationships between coal structures and combustion characteristics: The insights from micro-Raman spectroscopy based on 32 kinds of Chinese coals. *Appl. Energy* **2018**, *212*, 46–56. [CrossRef]
18. Vidano, R.P.; Fischbach, D.B.; Willis, L.J.; Loehr, T.M. Observation of Raman band shifting with excitation wavelength for carbons and graphites. *Solid State Commun.* **1981**, *39*, 341–344. [CrossRef]
19. Sadezkya, A.; Muckenhuberb, H.; Grotheb, H.; Niessnera, R.; Pöschla, U. Raman microspectroscopy of soot and related carbonaceous materials: Spectral analysis and structural information. *Carbon* **2005**, *43*, 1731–1742. [CrossRef]
20. Matthews, M.J.; Pimenta, M.A.; Dresselhaus, G.; Dresselhaus, M.S. Origin of Dispersive Effects of the Raman D Band in Carbon Materials. *Phys. Rev. B* **1999**, *59*, R6585. [CrossRef]
21. Cuesta, A.; Dhamelincourt, P.; Laureyns, J.; Martínez-Alonso, A.; Tascón, J.M.D. Raman microprobe studies on carbon materials. *Carbon* **1994**, *32*, 1523–1532. [CrossRef]
22. Rantitsch, G.; Bhattacharyya, A.; Schenk, J.; Lünsdorf, N. Assessing the quality of metallurgical coke by Raman spectroscopy. *Int. J. Coal Geol.* **2014**, *130*, 1–7. [CrossRef]
23. Xu, J.; Liu, J.; Zhang, X.; Ling, P.; Xu, K.; He, L.; Su, S.; Wang, Y.; Hu, S.; Xiang, J. Chemical imaging of coal in micro-scale with Raman mapping technology. *Fuel* **2020**, *264*, 116826. [CrossRef]
24. Tselev, A.; Ivanov, I.N.; Lavrik, N.V.; Belianinov, A.; Jesse, S.; Mathews, J.P.; Mitchell, G.D.; Kalinin, S.V. Mapping internal structure of coal by confocal micro-Raman spectroscopy and scanning microwave microscopy. *Fuel* **2014**, *126*, 32–37. [CrossRef]
25. Sforna, M.C.; Zuilen, M.; Philippot, P. Structural characterization by Raman hyperspectral mapping of organic carbon in the 3.46 billion-year-old Apex chert, Western Australia. *Geochim. Et Cosmochim. Acta* **2014**, *124*, 18–33. [CrossRef]
26. Seong, H.; Boehman, A.L. Evaluation of Raman Parameters Using Visible Raman Microscopy for Soot Oxidative Reactivity. *Energy Fuel* **2013**, *27*, 1613–1624. [CrossRef]
27. Liu, X.; Zheng, Y.; Liu, Z.; Ding, H.; Huang, X.; Zheng, C. Study on the evolution of the char structure during hydrogasification process using Raman spectroscopy. *Fuel* **2015**, *157*, 97–106. [CrossRef]
28. Dong, S.; Paterson, N.; Kazarian, S.G.; Dugwell, D.R.; Kandiyoti, R. Characterization of Tuyere-Level Core-Drill Coke Samples from Blast Furnace Operation. *Energy Fuels* **2007**, *21*, 3446–3454. [CrossRef]
29. Zhang, X.; Zou, C.; Zhao, J.; Ma, C.; Hu, B.; Liu, S.; He, J. Effect of H_2 and CO as pyrolysis atmosphere on chemical structure of char by XRD and Raman methods. *J. Fuel Chem. Technol.* **2019**, *47*, 1288–1297.
30. Rantitsch, G.; Bhattacharyya, A.; Günbati, A.; Schulten, M.; Schenk, J.; Letofsky-Papst, I.; Albering, J. Microsturctural evolution of metallurgical coke: Evidence from Raman spectroscopy. *Int. J. Coal Geology* **2020**, *227*, 103546. [CrossRef]
31. Wang, Y.; Alsmeyer, D.C.; McCreery, R.L. Raman Spectroscopy of Carbon Materials: Structural Basis of Observed Spectra. *Chem. Mater.* **1990**, *2*, 557–563. [CrossRef]
32. Jawhari, T.; Roid, A.; Casado, J. Raman spectroscopic characterization of some commercially available carbon black materials. *Caron* **1995**, *33*, 1561–1565. [CrossRef]
33. Dong, M.; Lu, J.; Yao, S.; Li, J.; Li, J.; Zhong, Z.; Lu, W. Application of LIBS for direct determination of volatile matter content in coal. *J. Anal. At. Spectrom.* **2011**, *26*, 2183–2188. [CrossRef]
34. Zhang, S.; Min, Z.; Tay, H.; Asadullah, M.; Li, C. Effects of volatile–char interactions on the evolution of char structure during the gasification of Victorian brown coal in steam. *Fuel* **2011**, *90*, 1529–1535. [CrossRef]
35. Babu, V.S.; Seehra, M.S. Modeling of disorder and X-ray diffraction in coal-based graphitic carbons. *Carbon* **1996**, *34*, 1259–1265. [CrossRef]